Cross-fringe versus single-fringe probabilities

W. Qin[1], P. Fraundorf[2]

[1] Technology Solutions, Freescale Semiconductor, Inc.
[2] Department of Physics and Astronomy and Center for Molecular Electronics, University of Missouri-St. Louis, St. Louis, MO 63121

High-resolution TEM is well-suited to characterizing nanocrystals, where lattice fringes serve as a source of structural information [1, 2]. For example, 3D lattice parameters can be measured from 2D lattice fringe images taken at as few as two different specimen orientations [3-6]. Recent work has shown that lattice fringe-visibility maps, a thin-specimen extension of bend-contour and channeling-pattern maps, can assist crystallographic study in direct space much as do Kikuchi maps in reciprocal space [7]. For example with lattice resolution and a sufficiently precise multi-axis goniometer, a nanocrystal can be tilted while the condition for visualizing a set of lattice fringes is maintained so as to "acquire" new lattice fringe normals (co-vectors) and thus continually refine a basis triplet containing information on both the nanocrystal's lattice and its orientation. Local specimen thickness measurements are another promising possibility.

Probabilities inferred from fringe-visiblity maps further allow one to examine the abundance of fringes in collections of randomly-oriented nanoparticles. In the thin-specimen limit, fringe-visibility bands have thickness proportional to d/t, rather than the λ/d proportionality expected for large t, where d is the lattice spacing, t is specimen thickness, and λ is electron wavelength. This follows from the expression for bandwidth half-angle at arbitrary thickness:

$$\alpha_{\max} = \sin^{-1}\left[\frac{df}{t} + \frac{\lambda}{2d}\left(1 - \left(\frac{df}{t}\right)^2\right)\right], \qquad (1)$$

where f is a "visibility factor" on the order of 1 that empirically accounts for signal-to-noise in the method used to detect fringes [7]. It's easy to see that the first term in (1) dominates for $t < 2\ d^2\ f/\lambda$ and therefore in typical transmission electron microscopes for inter-atom spacings in particles 10[nm] in size and smaller.

Fig. 1 shows the {200}, {111} and {220} fringe-visibility bands of a spherical f.c.c. nanocrystal. The probability of the (hkl) lattice plane to show fringes (e.g. in a HR-TEM image able to transfer projected-potential contrast in the d_{hkl} size range) is therefore that fraction of the solid angle subtended by the corresponding visibility band, i.e. $p_{(hkl)} = \sin[\alpha_{max}] \cong d_{hkl}f/t$ in the thin-specimen limit. Band intersections correspond to regions of visible cross-fringes. Successful calculation of the exact area of an intersection between visibility bands [7] indicates that flat-polygon intersection areas are an excellent small-angle approximation, in some cases with errors on the order of α_{max}^6. In this approximation, therefore, predicting the relative visibility of cross-fringes versus single fringes in a collection of randomly-oriented nanoparticles becomes a simple exercise in plane geometry. For example, the probability of cross-fringes from lattice planes 1 and 2, whose fringe-visibility bands have half-widths α_1 and α_2 and intersect at angle ϕ, is approximately the area of the suitable parallelogram over 4π, or $p_{1\times2} = 2\alpha_1\alpha_2/(\pi \sin\phi)$.

Figure 2 illustrates the fraction of randomly-oriented fcc particles showing only un-crossed (111) fringes, and the fraction of particles showing <110> zone cross-fringes assuming that both (111) and (200) spacings are detectable in suitably oriented grains. As you can see, cross-fringe grains become more abundant than single-fringe grains as grain diameter t decreases below 3[nm] because zone areas increase as $(df/t)^2$ while single-fringe regions increase in width as (df/t) and decrease in length at the expense of the zones. This model suggests, moreover, that the crossover size is quite sensitive to the visibility factor f for a given microscope/specimen combination. Figures 3 and 4 show how zone axis (cross-fringe) areas change as smaller spacings become reliably visible, as well as how fringe intensities in direct space mirror spot intensities in reciprocal space as an indicator of beam-specimen orientation.

References:

1. S.-C.Y. Tsen, P. A. Crozier, J. Liu, Ultramicroscopy 98(2003)63-72.
2. J. O. Malm, et al., Ultramicroscopy 68(1997)13.
3. P. Fraundorf, Ultramicroscopy 22(1987)225

4. P. Moeck, Verfahren zur Durchführung und Auswertung von elektronenmikroskopischen Untersuchungen, German patents DE 4037346 A1 and DD 301839 A7, priority date: 21 November, 1989.
5. W. Qin and P. Fraundorf, Ultramicroscopy 94(2003)245-262
6. W. Qin, Direct Space (Nano)crystallography via High-resolution TEM, Thesis, UM-StL/Rolla, 2000
7. P. Fraundorf et al., Making sense of nanocrystal lattice fringes, arXiv:cond-mat/0212281 (2005).

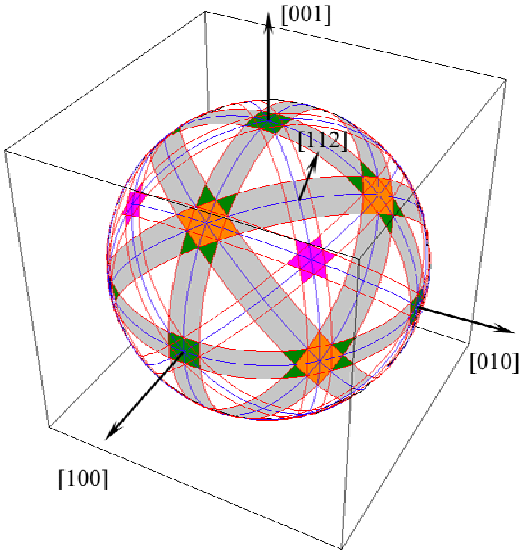

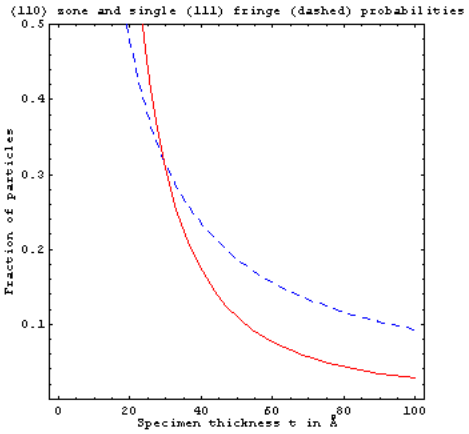

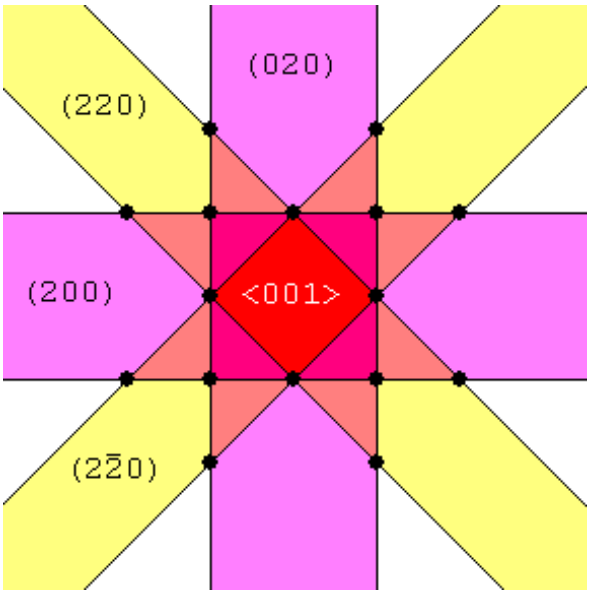

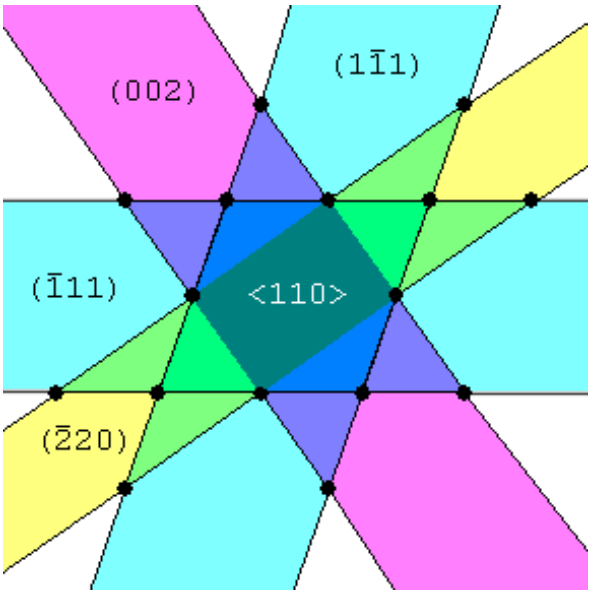

Figure 1 (upper left): The {200}, {111} (both shaded) and {220} (not shaded) fringe-visibility bands of a spherical f.c.c. nanocrystal.
Figure 2 (upper right): The reversal in relative abundance for cross-fringe versus single-fringe particles as a function of particle diameter.
Figure 3 (lower left): Polygonal cross-fringe zones for fcc ⟨001⟩ in the thin-specimen/small-angle approximations, built up as first {200} and then {220} fringes become visible. Note: the d/t dependence of bandwidth means that higher harmonics will reside within the existing bands.
Figure 4 (lower right). Polygonal cross-fringe zones for fcc ⟨110⟩ in the thin-specimen/small-angle approximations.